IOP Publishing New J. Phys. 26 (2024) 023022 https://doi.org/10.1088/1367-2630/ad1e90

New Journal of Physics
The open access journal at the forefront of physics

Deutsche Physikalische Gesellschaft DPG
IOP Institute of Physics

Published in partnership with: Deutsche Physikalische Gesellschaft and the Institute of Physics

OPEN ACCESS

RECEIVED
2 July 2023

REVISED
3 January 2024

ACCEPTED FOR PUBLICATION
15 January 2024

PUBLISHED
12 February 2024

PAPER

Towards the generation of mechanical Kerr-cats: awakening the perturbative quantum Moyal corrections to classical motion

Rodrigo G Cortiñas

Department of Applied Physics and Physics, Yale University, New Haven, CT 06520, United States of America
Yale Quantum Institute, Yale University, New Haven, CT 06520, United States of America

E-mail: rodrigo.cortinas@yale.edu

Keywords: Kerr oscillator, KPO, Groenwold's product, Kerr-cat qubit, laser tweezer, cold atoms, Moyal bracket

Abstract

The quantum to classical transition is determined by the interplay of a trio of parameters: dissipation, nonlinearity, and macroscopicity. Why is nonlinearity needed to see quantum effects? And, is not an ordinary pendulum quite nonlinear already? In this manuscript, we discuss the parameter regime where the dynamics of a massive oscillator should be quantum mechanical in the presence of dissipation. We review the outstanding challenge of the dynamical generation of highly quantum mechanical cat states of a massive 'pendulum', known as Kerr-cats. We argue that state-of-the-art cold atom experiments may be in a position to reach such a nonlinear regime, which today singles out superconducting quantum circuits. A way to stabilize Schrödinger cat superpositions of a mechanical atomic oscillator via parametric squeezing and further protected by an unusual form of quantum interference is discussed. The encoding of a neutral atom Kerr-cat qubit is proposed.

Different systems undergo the quantum to classical transition at different timescales and for different reasons [1, 2]. Many analogies between them can be made, nonetheless. The most relevant one may be the analogy that exists between mechanical systems, originally the focus of quantum *mechanics*, and electrical circuits. Quantum circuits made out of Josephson junctions are highly nonlinear, highly controllable and yet highly non-dissipative, and were used to test many quantum mechanical predictions [3–6] that are, to this day, impossible to access with mechanical systems. Yet, as high-precision experimental science advances it is important to establish the regime of validity of these analogies. For example, mechanical oscillators may suffer from gravitational decoherence while their electronic analogs, having otherwise the same Hamiltonian structure, will probably not.

A typical way to create quantum states in an oscillator, mechanical or not, is to use a two-level (nonlinear) ancilla to apply conditional 'forces' to a (linear) oscillator. This ancilla may be an internal [7–10] or external [11–14] degree of freedom of the oscillator, yet always entering as an external tensorial product in the description and requiring the buildup of entanglement. The oscillator can be then thought of as undergoing the entangled superposition of two different *classical dynamics*. An alternative to this is to use an unconditioned nonlinear oscillator to observe purely *quantum dynamics*. That is the deviations of the Schrödinger equation from Hamilton's classical equations of motion.

The minimalist example of these deviations is given by the refocusing of the phase in a Kerr oscillator [15], originally proposed for nonlinear crystals in laser optics [16]. In a quantum Kerr oscillator, a semiclassical coherent state $|\alpha\rangle$ will spread over phase space coherently, losing its phase before regaining it in a periodic manner. To the best of our knowledge, this purely quantum effect has only been observed in superconducting circuits [5, 17], where the role of *mechanical* momentum ($\hat{P}$) and position ($\hat{X}$) is played by the *electric* charge $\hat{Q} = \int \mathrm{d}t\hat{I}$ and flux $\hat{\Phi} = \int \mathrm{d}t\hat{V}$ degrees of freedom of the circuit (see, however, [18, 19]). Here $\hat{I}$ and $\hat{V}$ are the macroscopic current and voltage of the circuit, and the integral is over time [20].

In this manuscript, we will be interested in the experimental feasibility of testing the dynamics of a massive Kerr oscillator in this quantum regime. This regime requires the incursion into challenging experimental conditions: extreme nonlinearities are needed to awaken the quantum corrections to the

Poisson bracket which, in turn, are particularly sensitive to dissipation. Here, we distinguish the system's size, measured by its mass, from its quantum state macroscopicity, a measure related to the excitation number in the oscillator, and discuss how their interplay determines the effective rate of quantum nonlinear evolution, as well as the decoherence rate. The competition between these two rates determines the nature of the dynamics to be either classical or quantum, even when the system is effectively dissipationless i.e. we point to the emergence of frictionless classical physics from dissipative quantum mechanics in this system. This section of the manuscript is inspired by results reported across many disciplines [1–3, 16, 21–26].

Finally, elaborating on results reported in [17, 27–32], we discuss how to parametrically modulate the oscillator into a bifurcation that allows the encoding and control of a mechanical Kerr-cat qubit.

Dynamics in the quantum optical regime– Let us consider the evolution of an oscillator under ordinary dissipation [15, 33]. It can usually be described by the Lindblad equation $\partial_t\hat{\rho} = \frac{1}{i\hbar}[\hat{H},\hat{\rho}] + \kappa(\hat{a}\hat{\rho}\hat{a}^\dagger - \frac{1}{2}\left(\hat{a}^\dagger\hat{a}\hat{\rho} + \hat{\rho}\hat{a}^\dagger\hat{a}\right))$, where $\hat{\rho}$ is the density operator describing the oscillator's state, $\hat{H}$ is the oscillator's Hamiltonian operator, and $\hat{a} = \frac{1}{\sqrt{2}}(\hat{x} + i\hat{p})$, with $[\hat{x},\hat{p}] = i$, is the bosonic annihilation operator. The first term, involving the commutator, is the Schrödinger equation of motion, while the second term ($\propto \kappa$, the single photon loss rate) accounts for the nonunitary dynamics in the high quality factor (underdamped) regime [34].

At this point, an important step has already been taken: the nondimensionalization of the canonically conjugated position $\hat{X}$ and momentum $\hat{P}$ coordinates ($[\hat{X},\hat{P}] = i\hbar$). The formulation in terms of the bosonic operator $\hat{a}$ requires the introduction of a spatial metric and a momentum metric to reduce the dimensionful coordinates. We proceed, as is usual, by making the assumption of a weakly nonlinear system, characterized (in part) by its small oscillation frequency ω_o, and its mass m. The dimensionless coordinates read then $\hat{x} = \hat{X}/\sqrt{2}X_{\text{zps}}$ and $\hat{p} = \hat{P}/\sqrt{2}P_{\text{zps}}$ where $X_{\text{zps}} = \sqrt{\hbar/2m\omega_o}$ and $P_{\text{zps}} = \sqrt{\hbar m\omega_o/2}$ are the zero point spread of each coordinate. By introducing these metrics we have defined the *photon* (or phonon): a displacement in phase space by either $2X_{\text{zps}}$ or $2P_{\text{zps}}$ corresponds to a displacement by 'one photon' [35], for example.

This description based on Hilbert space operators obscures the connection to classical physics, and thus the study of decoherence. To bring the quantum description to the usual playground of classical physics we turn to the phase space formulation of quantum mechanics (see [36, 37]). For this, we consider the Wigner transform $\mathfrak{W}$ which transforms the Hilbert space density operator $\hat{\rho}$ to a phase space function called the Wigner function $W(x,p) = \mathfrak{W}(\hat{\rho})$.

The calculation of the equations of motion for the Wigner function is elementary if one uses that the *Hilbert space* product of operators maps, in an invertible manner, to Groenwold's *phase space* star-product $\mathfrak{W}(\hat{F}\hat{G}) = \mathfrak{W}(\hat{F}) \star \mathfrak{W}(\hat{G})$ [37]. It is defined to be the exponential of the Poisson bracket over the phase space functions $f(x,p) = \mathfrak{W}(\hat{F})$ and $g(x,p) = \mathfrak{W}(\hat{G})$ as [38]

$$f \star g \equiv f e^{\frac{i}{2}\left(\overleftarrow{\partial}_x\overrightarrow{\partial}_p - \overleftarrow{\partial}_p\overrightarrow{\partial}_x\right)} g \tag{1}$$

$$= fg + \frac{i}{2}\{f,g\} + \cdots . \tag{2}$$

The Lindblad equation then transforms to

$$\partial_t W = \{\{H,W\}\} + \frac{\kappa}{2}\left(\partial_x x + \partial_p p + \frac{1}{2}\left(\partial_x^2 + \partial_p^2\right)\right) W. \tag{3}$$

Here $H(x,p) = \mathfrak{W}(\hat{H}/\hbar)$ is the quantum Hamiltonian function (in units of angular frequency), and $\{\{H,W\}\} = \mathfrak{W}(\frac{1}{i\hbar}[\hat{H},\hat{\rho}])$ is the star-commutator and is known as the Moyal bracket.

Note the symmetry between ∂_x and ∂_p in equation (3). This is typical of a quantum optical treatment that distributes evenly the losses between both coordinates, even if microscopic models associate losses to only one of the coordinates [39]. This approximation is transparently explained in [23], for example, and it is valid essentially whenever the rotating wave approximation can be invoked. More refined models are possible [40] and oftentimes necessary [41], especially when considering physical implementation and when low-frequency classical control noise is the limiting factor. In this manuscript, we will however sustain the discussion at the level of photon loss ($\hat{a}$) as the decay mechanism since it provides a valuable effective model. General decoherence processes increase entropy by producing the incoherent spread of the phase space distribution and single photon loss is a minimal model to describe this phenomenology (see appendix).

Nonlinear correction to classical dynamics– For a Hamiltonian operator of the form $\hat{H}/\hbar = \omega_a\hat{a}^\dagger\hat{a} + V(\hat{x})$ [42] the Moyal bracket over the dimensionless coordinates reads

$$\{\{H,W\}\} = \{H,W\} \tag{4}$$

$$+\sum_{m=1}^{\infty} \frac{\partial_x^{(2m+1)} V \partial_p^{(2m+1)} W}{(2m+1)!}, \tag{5}$$

were $V(x) = \mathfrak{W}(V(\hat{x}))$ and $\{H,W\} = \partial_x H \partial_p W - \partial_p H \partial_x W$. We make three observations at this point. Firstly, the dependence on $\hbar$ has dropped out of sight from the quantum corrections by virtue of working with dimensionless coordinates. This is desirable since the observable quantum to classical transition cannot depend on the magnitude of $\hbar$. After all, it is a constant of nature. Secondly, non-vanishing quantum corrections require a nonlinear potential function $V(x)$. As a corollary, systems submitted to linear forces (i.e. quadratic potentials) undergo strictly classical dynamics generated by the Poisson bracket. Lastly, the susceptibility of the quantum correction to the nonlinearity is given by the 'rugosity' of the Wigner function as measured here by its higher-order derivatives. As we now briefly remind the reader [2, 43], this rugosity is a measure of the macroscopicity of the state and of its susceptibility to decoherence.

Decoherence– under the simple model that interests us here, dissipation enters dominantly [23, 24] in the dynamics as a diffusive term ($\propto \partial_x^2 + \partial_p^2$). Its effect is to dissolve the fine structure of the Wigner function and, with it, the quantum corrections to the dynamics. In general, a quantum state confined to an action $A \gg \hbar$ will develop a sub-Planckian fine structure in phase space of typical scale $a = \hbar^2/A$ [44]. Its origin is a quantum interference effect which will be naturally smoothened out by dissipation (diffusion). This feeds back into the unitary dynamics generated by the Schrödinger equation reducing it, effectively, to the classical Liouville equation [24]. The condition, thus, to observe quantum dynamics generated by the $(2m+1)$th order nonlinearity is

$$g_{2m+1} |\partial_p^{(2m+1)} W| \gg \kappa |\left(\partial_x^2 + \partial_p^2\right) W|, \tag{6}$$

where $g_{2m+1} = \partial_x^{(2m+1)} V|_{\text{equilibrium}}$, and the vertical bars indicate the characteristic magnitude of the Wigner function's derivatives [45]. This formula expresses that, to witness high-order nonlinear quantum dynamics, the nonlinear rate of evolution needs to dominate over diffusion-induced decoherence. These can be conflicting requirements since both magnitudes scale with different order derivatives of a bounded and square-integrable function W, which are constrained to a hierarchy.

The effect of size– it is important, in this competition between nonlinearity and dissipation, the effect produced by the system's size (its mass, or more specifically, its zero point spread in position). If the original potential reads $V(X) = \sum_{l \geqslant 3} k_l X^l$, then the lth effective nonlinearity in dimensionless coordinates is $g_l = k_l (\sqrt{2} X_{\text{zps}})^l$, and since X_{zps} is typically a microscopic scale, the effective nonlinearity drops rapidly with its order l. This coefficient measures the nonlinearity at the scale of the zero point spread, and thereby its quantum effects. However, if the dissipative terms dominate, the Lindblad equation reduces to the classical Fokker–Planck equation [1, 24, 46]. The replacement of the Moyal bracket by the Poisson bracket in equation (3) is sometimes called the 'truncated Wigner approximation'.

All q-legged cats decohere at the same rate in a harmonic oscillator: $2\kappa|\alpha|^2$– to illustrate that, i) the phase space fine structure is mainly determined by the phase space action available, $A/\hbar$, and that ii) this scale determines the sensitivity to decoherence [47], we consider a few multi-legged Schrödinger cat states (i.e. superpositions of q semiclassical coherent states $|\alpha\rangle$) of the same mean photon number $|\alpha|^2$. In figure 1 we plot their purity,

$$\text{Tr}\left[\hat{\rho}^2\right] = \int \text{d}x\text{d}p \; W(x,p) \star W(x,p)\,, \tag{7}$$

$$= 2\pi \int \text{d}x\text{d}p \; W^2(x,p)\,, \tag{8}$$

as a function of time while evolving in a harmonic oscillator under single photon dissipation [48]. In equation (8) we have used the integral property of the star product [37] (see also [49]). Their purity decays at the same rate in all cases (with the exception of the $q = 1$ semiclassical coherent state, which remains pure at all times). The purity saturates at $\approx 1/q$, a signature that the q dimensional space of quasi-orthogonal coherent states (which are *pointer states* [2, 15]) spans the mixed states. This illustrates that decoherence acts here at a timescale much faster than the energy damping, which will ultimately bring all states to the vacuum state.

A concrete example of nonlinear dynamics: the Kerr oscillator– consider an ordinary pendulum or, for that matter, any oscillator with a quartic nonlinearity. Using first-order perturbation theory to describe the regime of small oscillations, we write its Hamiltonian as $\hat{H} = \hbar\omega_o \hat{a}^\dagger \hat{a} + k_4 \left(\frac{\hbar}{m\omega_o}\right)^2 \hat{x}^4 + \cdots \approx \hbar(\omega_a \hat{a}^\dagger \hat{a} + K \hat{a}^{\dagger 2} \hat{a}^2)$. This is the so-called Kerr Hamiltonian in quantum optics. Its effective nonlinearity ($\propto g_4$) is

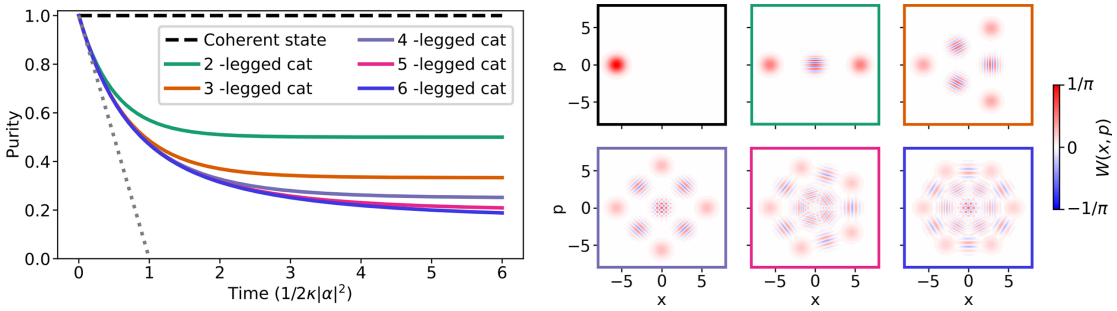

Figure 1. Decoherence of multi-legged cats with the same mean photon number $|\alpha|^2 = 16$. Left: purity as a function of time for a strictly harmonic oscillator initially prepared in a q-legged Schrödinger cat state with q ranging from one to six. The purity for all states decays at the same rate initially (as marked by the dotted line), with the exception of the $q = 1$ coherent which remains pure at all times. Right six panels: the Wigner function of the six initial states considered. The color of the frame references the time functions on the left plot. The interference pattern of these pure states, covering all of them the same phase space area (with the exception of the coherent state), have the same scale of fine structure, which makes them all decohere at the same rate. A similar relation between interference scale and decoherence can be seen in classical optics where, independently of the complexity of an interference pattern, the scale of the interference is set by the scale of the diffractive object. This interference scale sets the sensitivity of the pattern to perturbations [2, 44].

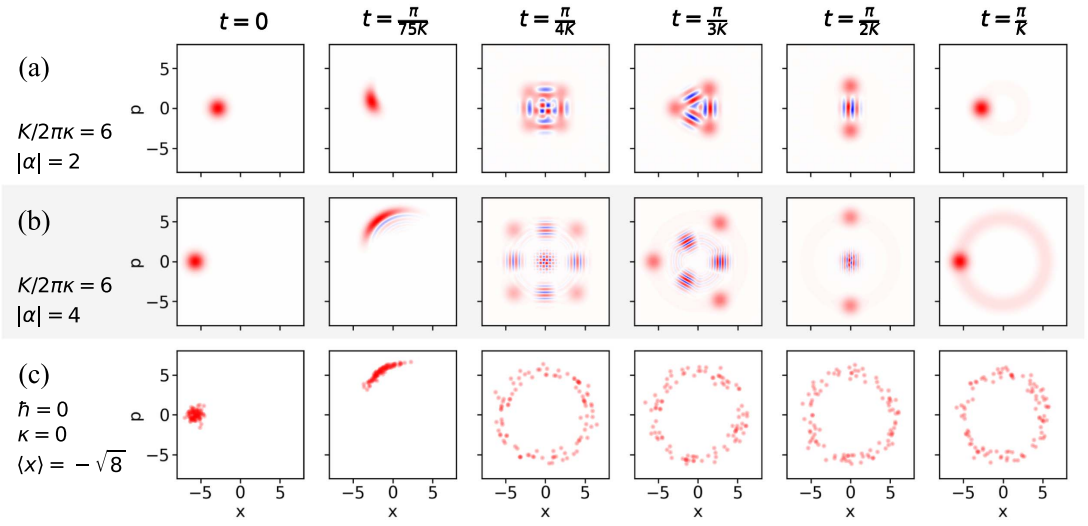

Figure 2. The quantum to classical transition. (a) A semiclassical coherent state with a mean photon number of $|\alpha|^2 = 2$ evolving under the Kerr Hamiltonian and weak damping. The Wigner distribution develops negativities (blue in color scale) as portions of the state interfere with each other. Schödinger cat states with q components form at $t = \pi/qK$. In (b) the initial state is larger ($|\alpha|^2 = 6$) and suffers accentuated decoherence. The refocusing of the phase at $q = 1$ has less contrast as the 'classical doughnut' emerges behind. Note that for $q > |\alpha|$, the coherent states will overlap significantly as they are equidistributed over a circle of radius $|\alpha|$ in phase space. They thus interfere among themselves generating nontrivial phase space distributions like the one shown for $t = \pi/75K$. Strictly speaking, we reserve the denomination 'q-legged cat states' for $2\pi|\alpha| \gg q > 1$. In (c), we plot the classical evolution analogous to (b) where the Moyal corrections to the Poisson bracket have been dropped. For this simulation, we solve Hamilton's equations for classical motion starting with a few infinitely localized initial classical states $W = \delta_{\text{Dirac}}(x, p)$ sampled from a Gaussian probability distribution centered at $\langle x\rangle = -\sqrt{2}|\alpha|$ and $\langle p\rangle = 0$ and a spread identical to that of the quantum case.

usually quoted as the Kerr coefficient $K = \frac{6k_4\hbar}{m^2\omega_o^2}$, and $\omega_a = \omega_o - 2K$ is the 'Lamb-shifted' oscillator frequency. The Kerr oscillator, also known as the Duffing oscillator in nanomechanics, has been extensively studied and we will here restrain ourselves to quote well-known results that can be found in the literature (see, for example, [15]).

This Hamiltonian has the outstanding property that it will turn a semiclassical coherent state $|\alpha\rangle$ into multilegged cats [15, 16] and will serve us well to study the quantum to classical transition in its simplest form. Going into the rotating frame at ω_a we bring the nonlinear dynamics into focus. In figure 2(a) we plot the phase space evolution of a coherent state in this reference frame for a series of times t, in presence of weak dissipation ($\frac{K}{2\pi\kappa} = 6$, which we regard as the nonlinear quality factor of the oscillator). We note that for $t = \pi/qK$ the system finds itself in a q-legged Schrödinger cat state. In particular, for $t = \pi/K$ the initial coherent state refocuses. In figure 2(b), we see how this coherent refocusing is degraded by increasing the mean number of excitations $|\alpha|^2$ (and thus the action) in the oscillator for the same value of $\frac{K}{2\pi\kappa}$. The

phaseless doughnut left behind is then more evident, and the refocusing has less contrast (see [5]). In figure 2(c), we show the frictionless classical evolution for an initially identical phase space distribution.

It is illuminating to quote and compare two different timescales involved in this problem which depend on the interplay of the parameter trio κ, K, and $|\alpha|^2$. Firstly, we note that the Kerr Hamiltonian preserves photon number and thus the phase space area covered by the evolution is bounded (by the total action). This means that all the cats generated during the evolution will have the same scale of fine structure in their Wigner function and thus decohere at a similar rate. For q-cats with mean photon number $|\alpha|^2$ the decoherence rate is given by $\Gamma_{\rm dcoh} = 2\kappa|\alpha|^2$, which is directly related to the high-frequency components (the rugosity) of their Wigner function [2, 15, 24, 44], and the single photon loss rate [50]. It is useful to understand the rate κ in this equation as the rate at which the radius of rotation (the doughnut's radius) is reduced, thus one sees that for $|\alpha|^2 \gg 1$ the quantum coherence is lost before the state suffers appreciable energy damping. Secondly, we consider the rate at which a semiclassical coherent state distribution develops phase space rugosity and negativities (interference fringes [15]) under the Kerr Hamiltonian. This is the rate at which nonlinear quantum effects become relevant and is given by $\Gamma_{\rm qnl} = 2|K||\alpha|/\pi$ [15]. Furthermore, this is also the rate at which the coherent distribution defocuses and it is proportional to the effective nonlinearity and to the square root of the mean excitation number.

These observations, together with the comparison of the three scenarios in figure 2, suggest that the classical regime appears in the limit $\kappa \to 0$, $|\alpha| \to \infty$ while $\kappa|\alpha| \gg |K|/2\pi$ (i.e. $\Gamma_{\rm dcoh} \gg \Gamma_{\rm qnl}$). In this sense, macroscopic states turn into a classical distribution almost immediately, at a timescale when the radius of rotation is unchanged and before the phase space rugosity and negativities develop [51]. In this limit, a *quantum dissipative* system naturally behaves as a *frictionless classical* system without the need to enforce Dirac's classical limit '$\hbar \to 0$' [2, 3]. Conversely, the macroscopic quantum dissipative regime, where fringes develop but there is barely any refocusing, is given by $\kappa \to 0$, $|\alpha| \to \infty$ and $\kappa|\alpha|^2 \gtrsim |K|/2\pi > \kappa|\alpha|$. Indeed, the condition for quantum dynamics reads $\Gamma_{\rm qnl} > \Gamma_{\rm dcoh}$, while the deep quantum regime is achieved for the more restrictive condition $|K|/2\pi \gg \kappa|\alpha|^2$ (i.e. $|K|/2\pi \gg \Gamma_{\rm dcoh}$), where many unitary cycles of defocusing and re-focusing of the phase take place before the distribution ultimately and unavoidably becomes classical.

We see then, that the essence of the quantum to classical transition can be found in the different scaling of $\Gamma_{\rm dcoh}$ and $\Gamma_{\rm qnl}$ with κ, K, and $|\alpha|^2$. From the scaling with $|\alpha|^2$, for example, we see that at fixed dissipative (κ) and nonlinear (K) rates, sufficiently macroscopic systems will be classical from the start.

Experimental scenarios and orders of magnitude– The minimalistic example of the Kerr oscillator provides analytical tools to compute the rates involved in a few model systems. We shall do so here to grasp the highly demanding regime of parameters required to observe these effects.

For an ordinary pendulum we have $\omega_o = \sqrt{g/l}$ and $k_4 = -g\frac{m}{4!l^3}$, where g, and l are the gravitational acceleration on earth's surface and the pendulum's length. Further, we take a mass $m = 1$ gram and $l = 10$ cm and compute $K/2\pi \approx -4 \times 10^{-31}$ Hz (independent of g). For a pendulum displacement of $l/10$ ($|\alpha| \approx 9.7 \times 10^{13}$), the quantum nonlinear timescale is $\Gamma_{\rm qnl}^{-1} \approx 6.1 \times 10^{15}$ s. At a frequency of a few Hertz and a quality factor $Q = \omega_o/2\pi\kappa$ of at most a few million, the oscillator will damp to vacuum well before nonlinear quantum effects arise ($\Gamma_{\rm dcoh} \gg \kappa = \frac{\omega_o}{2\pi Q} \gg \Gamma_{\rm qnl} \gg K/2\pi$). This is why bobs on strings, even when *almost* frictionless, appear classical in experience (see [1, 2]).

The next example we will discuss is that of a nanosphere trapped in optical tweezers. Assuming a one-dimensional Gaussian trapping potential [52] given by $V(X) = -V_0 e^{-2X^2/w_0^2}$, the small oscillation frequency and the nonlinearity are computed to be

$$\omega_o = \sqrt{\frac{4V_0}{mw_0^2}} \quad \text{and} \quad k_4 = -\frac{2V_0}{w_0^4}. \tag{9}$$

Considering state-of-the-art experimental scenarios [53, 54] we take $w_0 = 0.5$ μ m and a nanosphere of mass $m \approx 10^{-15}$ kg with a radius of $r \approx 50$ nm [55]. These conditions yield $K/2\pi \approx -2 \times 10^{-7}$ Hz (independent of V_0) and a defocusing time for a displacement of $w_0/10 \approx r$ ($|\alpha| \approx 10^5$ for $\omega_o/2\pi \approx 456$ kHz) of $\Gamma_{\rm qnl}^{-1} \approx 12$ s. If we can consider the limits imposed by the special theory of relativity [56] to bound $\kappa > 10^{-4}$ Hz ($Q < 7.3 \times 10^8$) we get $\Gamma_{\rm qnl}/\Gamma_{\rm dcoh} < 4 \times 10^{-8}$, which does not satisfy the condition derived above to develop quantum dynamics. From these arguments, we see also that high quality nonlinear nanomechanical resonators may be currently too massive, too dissipative and not sufficiently nonlinear for the observation of the focusing and refocusing of the phase during several periods $2\pi/K$ [57–61]. We would like to highlight, however, a recent achievement: the demonstration of a nonlinearity-boosting mechanism for a nanotube oscillator by coupling it with a quantum dot embedded in it [62]. In this experiment, the nonlinearity was sufficiently strong to be relevant at the scale of the zero-point spread of the nanotube and renormalize the frequency of the oscillator. This remarkable solid-state system shows the potential to reach the regime that interests us in this work.

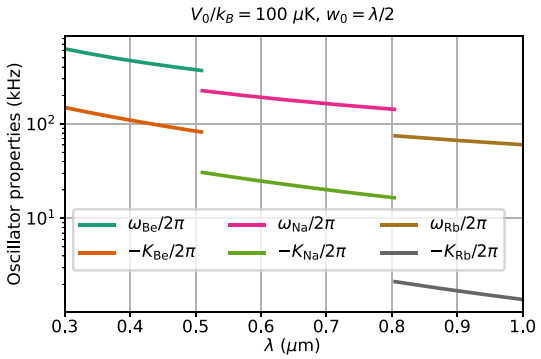

Figure 3. Radial potential properties for ^{9}Be, ^{23}Na, and ^{87}Rb trapped in a laser tweezer. We plot the properties equation (9) of a transversal oscillation of different atoms with respect to the beam propagation axis of a diffraction-limited (NA = 0.65) Gaussian trap of fixed depth $V_0/k_B = 100\ \mu$K. Note that the laser power needed to achieve this will be a strong function of the wavelength λ due to the dependence on the atomic polarizability. We plot the trapping range where trapping is practical for each species.

To conclude this section, we discuss the example of a ground-state Rubidium atom trapped in Gaussian optical tweezers in state-of-the-art experiments as in [63], for example. Typically one has the trapping laser beam focused to a waist of $w_0 = 1\ \mu$ m. We then get $K/2\pi \approx -350$ Hz. Yet, in these conditions, experimental quality factors in state-of-the-art atomic dipole traps remain at $Q \approx 10$ (see for example [64, 65]). Regardless, these laser traps are conservative and it is conceivable that they could reach $Q \approx 10^3$. We consider the case in which the atom state is initialized by a spatial displacement from its mechanical ground state of $w_0/8$ ($|\alpha| \approx 2$ for $\omega_{\rm Rb}/2\pi \approx 30$ kHz). In these conditions, we get $\Gamma_{\rm qnl}/\Gamma_{\rm dcoh} \approx \frac{|K|}{2\pi\kappa} \approx 1.8$, yet $\frac{|K|}{2\pi}/\Gamma_{\rm dcoh} \approx 0.22$ which may be enough to observe the effect but the conditions do not satisfy the requirements to be well within the quantum regime of dynamics.

Physics at the diffraction limit– note, that for the laser dipole trapping of an atom, the trap depth V_0 is directly proportional to the laser intensity (while the trap frequency $\omega_o \propto \sqrt{V_0}$) and to the electronic polarizability at the chosen laser wavelength λ [66] but that the Kerr nonlinearity is independent of the laser intensity. Yet, choosing smaller wavelengths allows one to get smaller diffraction-limited waists w_0 which will increase the nonlinearity as $K \propto w_0^{-2}$. Fixing the trap depth to $V_0/k_B = 100\,\mu$K, where k_B is the Boltzmann constant, we plot in figure 3 the trapping frequency ω_o and the Kerr nonlinearity K as a function of the laser wavelength assuming a beam focused to a diffraction-limited spot of $w_0 = \lambda/2$ (which corresponds to an objective lens with a numerical aperture of NA = 0.65 [67]), for a few atomic species in the regime were it is practically possible to trap them [68].

In spite of technical complications, laser trapping of atoms like Sodium atoms (^{23}Na), Lithium (^{7}Li) or even ions [69, 70] like Beryllium (^{9}Be$^+$), offer two advantages with respect to Rubidium: they are lighter and can be trapped with lasers of shorter wavelengths. Being lighter, the trap frequency and the zero point spread in position are increased at fixed trap depth. This improves the validity of the perturbative approach and the effective nonlinearity simultaneously. In the case of ^{9}Be$^+$, ion-trapping techniques could facilitate the preparation and cooling of the sample [71]. For Beryllium we consider $\lambda = 300$ nm and a displacement of $w_0/3$ (i.e. $|\alpha| \approx 2.1$, considering $\kappa = (10\ \text{ms})^{-1}$ (which for $\omega_{\rm Be}/2\pi \approx 500$ kHz yields $Q \approx 5 \times 10^3$), implies $\frac{|K|}{2\pi}/\Gamma_{\rm dcoh} \approx 170$. In fact, these conditions are so nonlinear that the perturbative Kerr approximation used so far [$\omega_o|\alpha|^2 \gg K|\alpha|^4$ (independent of trap depth)] needs to be carried out to higher order to correctly capture the quantum dynamics of this oscillator. Thus, we see that the quantum optical regime where $\frac{|K|}{2\pi}/\Gamma_{\rm dcoh} \gg 1$ at the single photon (or phonon) level ($|\alpha| \gtrsim 1$) as in [5] should be observable in the mechanical motion of the atom if sufficiently high quality factors can be achieved.

Decoherence snapshots of mechanical Schrödinger Kerr-cats could be obtained by adapting recent techniques reported in [64]. This would constitute a foundational test of quantum mechanics complementary to seminal results reported in [3, 5] on electrical superconducting systems and it will open pathways to encode quantum information in the mechanical mode of a laser-trapped cold atom [72, 73] at room temperature (see below).

On the observation of mechanical Kerr-cats– even if the full time-resolved experimental tomography of the Wigner function, that will yield images similar to those shown in figure 2, is an unparalleled visualization tool [3, 5], it may be prohibitively costly with current technological means. The information reflecting the generation of the mechanical Kerr-cats, however, can be accessed via more economical partial observables. As an example we discuss the possibility to measure, using standard time-of-flight techniques [74], the position of the atom [75]. In the quantum optical regime, the signal will show a characteristic and detectable beating

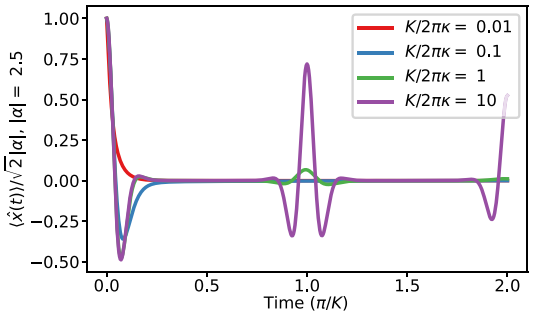

Figure 4. Observable prediction for the quantum mechanical motion of an atom. Coherent quantum dynamics present, as a general feature, periodic oscillations when the state is spanned by a finite number of states with commensurate eigenenergies. In the case of the Kerr oscillator, this is also true for any infinite superposition. This is due to the quadratic energy distribution $E_N = \hbar KN(N-1)$ (which is always an even multiple of $\hbar K$). With period π/K [15], all accumulated phases are a multiple of 2π and the initial state refocuses. Here we show an example of dynamics for the system initialized in a coherent state ($\alpha = 2.5$). We show how an increasing ratio κ/K erases the coherent periodicity, which otherwise directly reveals the energy quantization of the nonlinear oscillator. The observable is here described in the rotating frame at ω_a. The blue curve corresponds to an overdamped system. The orange curve corresponds to Newtonian mechanics [34] and the abstraction of a 'dissipationless system' but not sufficiently so to exhibit quantum mechanical behavior (see figure 2(c) and main text). The green and red curves exhibit quantum mechanical revivals with different degrees of contrast (see figure 6).

pattern. The signal will have a distinct Fourier composition corresponding to the Fock states spanning the initial coherent state $|\alpha\rangle = e^{-\frac{|\alpha|^2}{2}} \sum_{N=0}^{\infty} \frac{\alpha^N}{\sqrt{N!}} |N\rangle$. Each of them at a frequency $E_N/\hbar = KN(N-1)$. In figure 4, we show the mean value of the position function $\langle \hat{x}(t) \rangle$, for $\alpha = 2.5$, and for different values of the nonlinear quality factors of the oscillator. For $K/2\pi\kappa = 10$, the phase revivals are conspicuous. For $K/2\pi\kappa = 0.01$, the quantum Lindblad equation yields a result similar to a classically overdamped nonlinear oscillator, and for $K/2\pi\kappa = 0.1$, we see what we would expect from figure 2(c): a classical oscillator with weak or no damping.

Driven dynamics: the stabilization of a cat qubit in the mechanical motion of a neutral atom– Once a highly nonlinear mechanical oscillator is available other tests can be made. As an example with far-reaching consequences, we will now discuss the interplay between different types of photon (or phonon) 'interactions'. The Kerr effect can be understood as an interaction energy in between photons [76, 77] as the energy contribution is written $\hat{a}^{\dagger 2}\hat{a}^2 = \hat{n}(\hat{n}-1)$, which counts the pairs of bosons available. Hamiltonian squeezing, on the other hand ($\propto (\hat{a}^{\dagger 2} + \hat{a}^2) = \hat{x}^2 - \hat{p}^2$), is an interaction that creates or destroys bosons in pairs and it has an unbounded spectrum without a ground state. Their interplay generates nontrivial dynamics as we will now remind the reader [27, 29, 30, 32, 78, 79].

Considering the Gaussian potential to first nontrivial order we write

$$V(X) = k_2 X^2 + k_4 X^4 + \cdots . \tag{10}$$

In dimensionless units, one has

$$V(x) = \frac{\hbar}{4}\sqrt{\frac{4V_0}{mw_0^2}}x^2 - \frac{\hbar^2}{8mw_0^2}x^4 + \cdots . \tag{11}$$

We now define the complex notation of the phase space coordinates as $a = \frac{1}{\sqrt{2}}(x + ip)$ which we can use to re-write the potential above before we apply perturbation theory. At this point, an important decision should be made about the nature of the problem: should $(a + a^*)^4$ be understood as an ordinary commutative multiplication of phase space functions or as $\star$-multiplication? The latter corresponds to the quantum description of the problem, which transforms to Hilbert space via the inverse Wigner transform $\mathfrak{W}^{-1}(V)$ as

$$\hat{V} = \frac{\hbar}{8}\sqrt{\frac{4V_0}{mw_0^2}}\left(\hat{a} + \hat{a}^\dagger\right)^2 - \frac{\hbar^2}{32mw_0^2}\left(\hat{a} + \hat{a}^\dagger\right)^4 + \cdots . \tag{12}$$

Here we wrote $\mathfrak{W}^{-1}(a) = \hat{a}$ [37].

Naturally, the different choices will yield different predictions for the dynamics. In the simple case of Kerr and squeezing, the differences will manifest as directly observable differences of the Hamiltonian parameters. As we will see, under a squeezing drive a Kerr oscillator can undergo a bifurcation. The prediction for the location of that bifurcation in parameters space, as well as the system's rich dynamics, depend on the choice

of product to be made. Higher-order nonlinear processes will instead yield more drastic divergence in the quantum and classical predictions. For an in-depth discussion of this divergence of quantum and classical highly nonlinear driven processes, we refer the reader to [77]. For a more pedagogical discussion, an example based on the Kapitza pendulum is discussed in detail in the appendix of [80].

Noting that the nonlinear term is independent of the trap depth V_0, we consider the time-dependent parametric driving condition $V_0 \to V_0 + F\cos(\omega_d t)$ over the harmonic part of the potential. Considering $\omega_d - 2\omega_o \ll \omega_o$ and $F \ll V_0$ brings the problem to the conditions already theoretically studied in [27–30, 78, 81, 82], where the oscillator becomes bi-stable. The bifurcation is the same physical process suffered by a kid in a swing when moving up and down its center of mass to stabilize one of two possible oscillations. To perform the usual time-dependent perturbation theory, we exhibit the explicit linear time-dependence of the coordinates as $a \to ae^{i\omega_o t}$, and write the quadratic Hamiltonian term as

$$\approx \left(\sqrt{V_0} + \frac{F}{2\sqrt{V_0}}\frac{e^{i\omega_d t} + e^{-i\omega_d t}}{2}\right)\left(ae^{i\omega_o t} + a^* e^{-i\omega_o t}\right)^2 \tag{13}$$

$$\approx \sqrt{V_0}a^* a + \frac{F}{4\sqrt{V_0}}\left(a^2 + a^{*2}\right), \tag{14}$$

where equation (14) corresponds to the rotating wave approximation [15, 81]. The full static effective Hamiltonian approximation, including the kinetic energy quadratic in the dimensionless momentum p and up to irrelevant constants, reads

$$\begin{aligned} H(x,p) &= \Delta a^* a + \epsilon_2\left(a^{*2} + a^2\right) - Ka^{*2} \star a^2 \\ &= \Delta'\left(x^2 + p^2\right) + \epsilon_2\left(x^2 - p^2\right) - \frac{K}{4}\left(x^2 + p^2\right)^2, \end{aligned} \tag{15}$$

where $\Delta = \omega_o - \omega_d/2 - 2K$ and $\epsilon_2 = F/4\sqrt{V_0}$ while K was defined earlier. In the quantum case one has $\Delta' = \omega_o - \omega_d/2 - K$ but in the classical case one has $\Delta' = \omega_o - \omega_d/2$. The difference can be considered a quantum 'Lamb shift' [80] arising from the noncommutativity of the quantum product. One sees that, regardless of this difference, there are two competing symmetries in this Hamiltonian. The squeezing term ($\propto \epsilon_2$) has a saddle structure in phase space, while the harmonic and nonlinear Kerr terms have revolution symmetry. The phase space Hamiltonian energy surface equation (15) thus describes a transition from a single well system to a double well system as ϵ_2 increases [32]. The location of the transition in parameter space is associated to the appearance of multiple solutions to $\partial_x H = \partial_p H = 0$. The prediction for the transition into the double well regime happens then for the drive condition

$$2\epsilon_2 = \Delta' = \begin{cases} \omega_o - \omega_d/2 - K & \text{Quantum,} \\ \omega_o - \omega_d/2 & \text{Classical.} \end{cases} \tag{16}$$

In other words, the difference is the Lamb shift between ω_o and ω_a. Note that ω_o can be directly measured by a profilometry of the laser trap intensity while ω_a is directly measured as the natural small oscillation frequency of the atoms in the trap.

Quite remarkably, driving a quantum system according to each of these two different prescriptions one obtains either a system that exhibits ground state tunneling between the two stable solutions [78] or not at all [29]. To show this, we consider the quantum corrections and take the drive's frequency to be $\omega_d = 2(\omega_o - 2K)$ in order to obtain the resonance condition $\Delta = 0$. Under this driving condition the Hamiltonian admits the factorization [29, 82]

$$H = -K\left(a^{*2} - \frac{\epsilon_2}{K}\right) \star \left(a^2 - \frac{\epsilon_2}{K}\right), \tag{17}$$

which, has a two-fold degenerate ground state, spanned by coherent states $|\pm\alpha\rangle$ with $\alpha = \sqrt{\epsilon_2/K}$ and with Wigner function $W_{\pm\alpha}(x,p) = \mathfrak{W}(|\pm\alpha\rangle\langle\pm\alpha|)$. This is seen by noting that $\{\{H, W_{\pm\alpha}\}\} = 0$, or moreover [37]

$$H \star W_{\pm\alpha} = 0. \tag{18}$$

That is, $W_{\pm\alpha}$ are $\star$-eigenfunctions of the Hamiltonian with eigenenergy zero [83]: the states are fundamentally degenerate and correspond to the ground states of the double well phase space surface defined by equation (15), with the peculiar property that the tunnel splitting is exactly zero [84]. Note that the degenerate ground state spanned by two coherent states can encode one qubit of information in Schrödinger cat superpositions [29, 85]. This has been originally proposed for trapped ions [27] but could only be

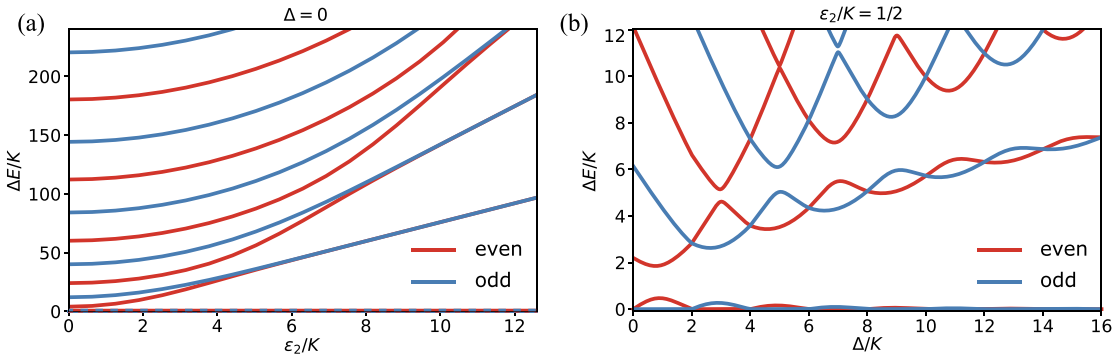

Figure 5. Exponential degeneracy and braiding. (a) Excited state static effective energies spectrum of a resonant ($\Delta = 0$) squeeze-driven Kerr oscillator as a function of ϵ_2/K.The depth of the wells is given by ϵ_2^2/K. A degenerate pair of ground states defined by equation (18) are at $\Delta E = 0$. The exponential pairwise approach of the static effective energies happens as the static effective states sink under the effective potential barrier [17, 28]. The color of the lines defines the parity of the eigenstate in the Fock basis. (b) Static effective energies as a function of Δ/K for $\epsilon_2/K = 1/2$. The crossings between states of different parity corresponds to the dynamical cancellation of tunneling (zeros of tunnel splitting) [30, 32]. A singly degenerate ground state is at $\Delta E = 0$ for all $\Delta/K \neq$ even. The singly degenerate ground state alternates between bonding (even) and antibonding (odd) superposition of the well states. For $\Delta/K = 2m$, m integer, the ground state becomes doubly degenerate and the spectrum shows a remarkable set of $m+1$ exact degeneracies [28, 31, 32].

demonstrated in superconducting circuits [86] two decades later. In the conditions here proposed, the qubit implementation in an atomic oscillator could be realized.

The driving condition such that $\omega_d = 2\omega_o$ will instead break the factorization condition, as well as the degeneracy, and induce a tunnel splitting predicted in [78].

Both these long-standing predictions of quantum optical tunneling in this driven Hamiltonian [30, 78] are yet unobserved in mechanical systems and were only recently observed in superconducting circuits [17, 32] where the voltage of a bifurcated electronic oscillator in the quantum regime was observed to tunnel between the stable states. In figure 5(a) we show the observable spectroscopic signature of this dynamical (driven) tunnel effect for $\Delta = 0$. Note the exponential suppression of tunnel splitting in the excited static effective states: as the squeezing term becomes more and more relevant, the wells get wider in phase space (enclosing more action) and able to hold more and more excited states within (the number of states per well is given by a semiclassical action-quantization theory to be $\epsilon_2/\pi K$ [17]), which in turn exponentially degenerate in energy as they sink under the barrier. Two energy levels fundamentally degenerate at $\Delta E = 0$ according to equation (18) are present. Furthermore, the tunneling in this Hamiltonian can be completely controlled *in situ* [32] by changing the drive parameter ω_d (linearly controlling Δ) due to a quantum coherent destruction of tunneling paths in the classically forbidden region predicted in [30] (see also [28, 31, 87]). This unusual effect originates in the relativistic-like p^4 term in the static effective Hamiltonian equation (15). This coherent destruction of tunneling (not to be confused with similar but fundamentally different phenomenology in [88–91]) is conspicuous from figure 5(b) where simultaneous spectral degeneracies between states of different parity appear in the ground and excited states when Δ/K takes even values. In fact, if $\Delta = 2mK$ with m an integer, it can be shown that the spectrum contained $m+1$ exact degeneracies, independent of the value of F or V_0 [28, 32]. The dynamical counterpart of these degeneracies is the exact cancellation of tunneling, which can be directly observed [64]. This rare interference effect in the classically forbidden region allows for yet another type of Schödinger cat qubit encoding with enhanced protection [31, 32] that could also be encoded in an atomic oscillator.

We note that this parametric bifurcation has been observed for laser-levitated nanoscopic oscillator [53] but the experiment was constrained to the classical regime. Quantum tunneling and the energy level structure in figure 5 were then not observable. However, a different proposal to use a double well to exhibit quantum mechanical effects of a nanoparticle has been recently proposed [92].

Discussion and concluding remarks– to the best of our knowledge, the dynamical generation of Kerr-cats has only been observed in superconducting circuits. The pioneering experiment, demonstrating the generation of these electric Kerr-cats, was reported a decade ago in [5]. A study as a function of the system's macroscopicity (understood here as the excitation number in these cats) is reported in [17] [there, $\kappa^{-1} = 20\,\mu$s, $K/2\pi = 320$ kHz and $\omega_a/2\pi = 6$ GHz and $|\alpha|^2 < 10$ — these conditions correspond to figures 2(a) and (b)].

Pioneering experiments with 'ions and phonons' [7] and 'Rydberg atoms and photons' [11] in the 90s were the first to show that effective nonlinearities can be induced on a harmonic oscillator if dressed by a two-level atom [93]. That is, the generation of the quantum state was achieved by quantum-conditional

linear dynamics (rotations or displacements that are Gaussian operation [94]) generated by the Poisson bracket. We stress, however, the difference between two classes of quantum effects, *quantum effects induced by the interaction between two quantum systems* (entanglement) and *a system which unconditionally and by itself will become quantum*. In the absence of dissipation, a displaced pendulum hanging from the roof should become a quantum superposition of cat states by itself [95]. The same is true for Hyperion, a moon of Saturn [1]. The dynamics discussed in this manuscript belong to the latter class and to the best of our knowledge, it has not been observed so far in mechanical systems.

The observation of these effects for a massive mechanical particle may be within reach for state-of-the-art cold atom experiments. The pursuit of the technology needed to observe these effects will bring insight into decoherence mechanisms limiting cold atom experiments in tweezers. This is important to understand the scopes of quantum technologies using neutral atoms, in particular, those involving Rydberg excitations in atomic tweezers arrays to perform quantum simulation and computation [96, 97]. In these systems, interaction-induced motion may produce damaging 'spin'-motion entanglement in nonlinear traps, producing non-Markovian decoherence in quantum simulators of spin chains [98], for example. Conversely, this entanglement could produce interesting quantum simulations of spin-Boson models [99]. The explicit introduction of bosonic nonlinearity in this model may be an interesting avenue for quantum simulation.

Note, that the analysis presented disregards other sources of informational decoherence [2, 100]. For example, the aforementioned atomic oscillators will suffer from heating due to the off-resonance scattering of laser photons, or due to laser intensity fluctuations. Importantly, however, these heating sources can be modeled as a first approximation as a renormalization of κ for sufficiently large cat states (see appendix) and are thus encompassed by the discussion here presented as merely producing a further reduction of the quality factor of the oscillator. In particular, the phenomenology of figure 2 remains unchanged if the initial state is a thermal distribution rather than a coherent state, provided that the initial displacement is larger than the thermal spread and the nonlinear quality factor remains large enough. Should the high quality factor regime in the mechanical motion of a laser-trapped atom be achievable, a new field of mechanics in the quantum optical regime will be available. This is especially important in the context of mechanical parametric processes [77] and chaos of an individual driven systems [91, 101–104].

In terms of applications, it was predicted that a Kerr oscillator in the quantum regime, when driven by parametric squeezing, could host an autonomously error-protected qubit in trapped ions [27] and circuits [29]. This encoding of quantum information was demonstrated in superconducting circuits and reported in [86] (see also [105]). The technology was named the *Kerr-cat qubit* since the bifurcated oscillator functions as a Hamiltonian stabilization for two-legged cat (ground) state superpositions. In this encoding, the free Kerr evolution discussed in figure 2 functions as a single-qubit Hadamard logical quantum gate. Extending the ideas put forward in this article to laser-trapped Rydberg atoms [106] in interaction may provide a mechanism for a two-qubit logical gate [107] enabling opportunities for fault-tolerant quantum computation [108]. Furthermore, the phenomenology at the one and two oscillator levels has direct implications for the study of ground [109] and excited state quantum phase transitions (ESQTP) [110–113] (see also [114]). As such, the mechanical motion of cold atoms in room temperature setups could incur into a technologically relevant regime where only highly nonlinear, low-dissipation superconducting quantum circuits operate today.

Data availability statement

No new data were created or analysed in this study.

Note added during editing

Recently a remarkable experiment using a squeezed vacuum state has been able to observe the quantum effects of the Kerr nonlinearity in an acoustic wave [https://arxiv.org/abs/2312.16169]. The effective mechanical nonlinearity is achieved by coupling to a superconducting qubit. The system scores $\frac{K}{2\pi\kappa} \sim 0.56$ and operates at a mean phonon number of $\sim$0.2.

Acknowledgments

R G C acknowledges and is grateful to M Devoret, J Venkatraman, X Xiao, and N Frattini for fruitful collaboration and discussions on topics closely related to this manuscript, to J-M Raimond, M Devoret for critics of an early version of this manuscript, and to A Bachtold, O Romero-Isart, M Aspelmeyer, M Dykman, L Santos, T Lahaye, M Frimmer, S Zacarias, N Navon, N Harle and C Regal for related discussions. Support from the Center for Quantum Dynamics on Modular Quantum Devices (NSF Grant No. CHE-2124511) and from the Yale Quantum Institute is gratefully acknowledged.

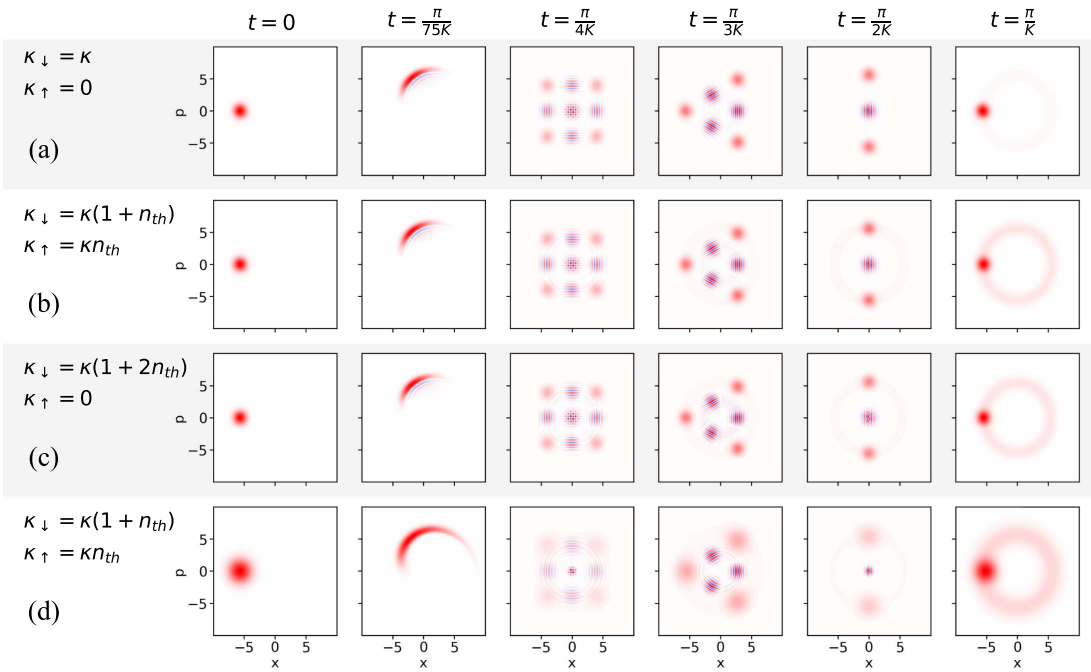

Figure 6. Decoherence of dynamical Kerr-cats in presence of temperature. We show snapshots of the Wigner function of Gaussian states under the Kerr Hamiltonian and Markovian single photon loss and gain, where $K/2\pi\kappa = 20$. In (a), we initialize the state in a coherent state ($\alpha = -4$) and set the thermal excitation rate (and stimulated emission rate) to zero for reference. In (b), we set thermal rates corresponding to nth $= 1$. In (c), we set $\kappa_\uparrow = 0$, and set $\kappa_\downarrow \to \kappa_{\rm eff} = 3\kappa$ for comparison with (b). In (d), the initial state is a thermal state (nth $= 1$) displaced by $\alpha = -4$, which evolves under thermal rates corresponding to $n_{th} = 1$.

Appendix

A.1. Dissipation and heating in the generation of Kerr-cats

The operator-valued Lindblad equation in presence of single photon loss and single photon gain reads

$$\partial_t\hat{\rho} = \frac{1}{i\hbar}\left[\hat{H},\hat{\rho}\right] + \kappa_\downarrow\mathcal{D}\left[\hat{a}\right]\hat{\rho} + \kappa_\uparrow\mathcal{D}\left[\hat{a}^\dagger\right]\hat{\rho}, \tag{19}$$

where $\mathcal{D}[\hat{O}]\hat{\rho} = \left(\hat{O}\hat{\rho}\hat{O}^\dagger - \frac{1}{2}\left(\hat{O}^\dagger\hat{O}\hat{\rho} + \hat{\rho}\hat{O}^\dagger\hat{O}\right)\right)$ defines the dissipator superoperator of the collapse operator $\hat{O}$. In a thermal environment [15] one has $\kappa_\downarrow = \kappa(1 + n\text{th})$, which accounts for spontaneous and thermal stimulated emission and $\kappa_\uparrow = \kappa n\text{th}$, which accounts for thermal excitation. Here nth represents the mean number of thermal photons and models the effect of temperature. It is straightforward to get its phase space counterpart using the definition of Groenwold's product and we refer the reader to [2, 17, 23, 24] for related discussions.

In figure 6, we show the effect of temperature in the quantum Kerr evolution [equation (19), with $\hat{H} = \hbar K\hat{a}^{\dagger 2}\hat{a}^2$] of Gaussian states. For these numerical simulations, we used $K/2\pi\kappa = 20$, a value larger than that of figure 2 in the main text, to make the effects directly related to temperature clear. In cases (a–c), the initial state is a coherent state with $\alpha = -4$. In figure 6(a), we set the thermal excitation rate to zero ($\kappa_\uparrow = 0$) as a point of reference. Correspondingly, the spontaneous emission rate is set to $\kappa_\downarrow = \kappa$. In figure 6(b), we set $\kappa_\downarrow = \kappa(1 + n\text{th})$ and $\kappa_\uparrow = \kappa n\text{th}$, with nth $= 1$. We see that the effect of temperature is to accelerate the effect of dissipation, reducing the refocusing contrast at $t = \pi/K$, and making the classical doughnut emerge earlier. In figure 6(b), which is remarkably similar to figure 6(c), we have set the thermal excitation rate to zero ($\kappa_\uparrow = 0$) but the spontaneous emission rate has been effectively enhanced to $\kappa_\downarrow \to \kappa_{\rm eff} = \kappa(1 + 2n\text{th})$, with nth $= 1$. That is, forcing $\hat{a}^\dagger \to \hat{a}$ in the master equation equation (19) is a good approximation in what concerns the quantum to classical transition in this system. The main difference between (b) and (c) is that for (b), the doughnut widens (thermal diffusion) while for (c), it mainly shrinks in radius.

Quite generically, regarding the decoherence caused by ordinary dissipation in an oscillator (equation (19)), the mechanism for the erasure of the phase space Wigner rugosity (the interference fringes) is the change of photon number parity caused by single photon loss and gain [15]. This is easiest to see using Schrödinger cat states as examples. For sufficiently large cats ($|\alpha|^2 \gtrsim 10$), losing or gaining a photon has little effect on their (mean) photon number, yet it does change the state parity (and thus the sign of the phase space

interference fringes [3, 15]). This comes from the fact that $\hat{a}|\alpha\rangle = \alpha|\alpha\rangle$ and $\hat{a}^\dagger|\alpha\rangle = \alpha^*|\alpha\rangle + \mathcal{O}(1/|\alpha|)$. So that $\hat{a}^\pm(|\alpha\rangle + e^{i\theta}|-\alpha\rangle) \propto |\alpha\rangle - e^{i\theta}|-\alpha\rangle$, and thus become orthogonal. Here, $\hat{a}^\pm$ is a shorthand notation for the bosonic creation and annihilation operators. Thus, the effect of adding photons is similar to that of losing photons in what respects to the coherence of Schrödinger cats states. Ultimately, the interference fringes with different signs will average out to zero, effectively erasing the quantum effects.

Finally, we show in figure 6(d) the evolution given by equation (19) for an initial thermal distribution ($n_{th} = 1$) displaced by $\alpha = -4$. We see that the generation of mechanical Kerr-cats, as evidenced by the emergence of the phase space interference pattern, does take place regardless of moderate heating.

References

[1] Zurek W H and Paz J P 1999 Why we don't need quantum planetary dynamics: decoherence and the correspondence principle for chaotic systems *Epistemological and Experimental Perspectives on Quantum Physics* (Springer) pp 167–77
[2] Zurek W H 2003 Decoherence, einselection and the quantum origins of the classical *Rev. Mod. Phys.* **75** 715
[3] Deleglise S, Dotsenko I, Sayrin C, Bernu J, Brune M, Raimond J-M and Haroche S 2008 Reconstruction of non-classical cavity field states with snapshots of their decoherence *Nature* **455** 510
[4] Wilson C M, Johansson G, Pourkabirian A, Simoen M, Johansson J R, Duty T, Nori F and Delsing P 2011 Observation of the dynamical casimir effect in a superconducting circuit *Nature* **479** 376
[5] Kirchmair G, Vlastakis B, Leghtas Z, Nigg S E, Paik H, Ginossar E, Mirrahimi M, Frunzio L, Girvin S M and Schoelkopf R J 2013 Observation of quantum state collapse and revival due to the single-photon kerr effect *Nature* **495** 205
[6] Minev Z K, Mundhada S O, Shankar S, Reinhold P, Gutiérrez-Jáuregui R, Schoelkopf R J, Mirrahimi M, Carmichael H J and Devoret M H 2019 To catch and reverse a quantum jump mid-flight *Nature* **570** 200
[7] Wineland D J 2013 Nobel lecture: superposition, entanglement and raising schrödinger's cat *Rev. Mod. Phys.* **85** 1103
[8] Gerlich S, Eibenberger S, Tomandl M, Nimmrichter S, Hornberger K, Fagan P J, Tüxen J, Mayor M and Arndt M 2011 Quantum interference of large organic molecules *Nat. Commun.* **2** 1
[9] Flühmann C, Negnevitsky V, Marinelli M and Home J P 2018 Sequential modular position and momentum measurements of a trapped ion mechanical oscillator *Phys. Rev.* X **8** 021001
[10] Keil M *et al* 2021 Stern-gerlach interferometry with the atom chip *Molecular Beams in Physics and Chemistry: From Otto Stern's Pioneering Exploits to Present-Day Feats* ed B Friedrich and H Schmidt-Böcking (Springer International Publishing) pp 263–301
[11] Haroche S 2013 Nobel lecture: controlling photons in a box and exploring the quantum to classical boundary *Rev. Mod. Phys.* **85** 1083
[12] Ofek N *et al* 2016 Extending the lifetime of a quantum bit with error correction in superconducting circuits *Nature* **536** 441
[13] Campagne-Ibarcq P *et al* 2020 Quantum error correction of a qubit encoded in grid states of an oscillator *Nature* **584** 368
[14] Bild M, Fadel M, Yang Y, von Lüpke U, Martin P, Bruno A and Chu Y 2022 Schrödinger cat states of a 16-microgram mechanical oscillator *Science* **380** 274–8
[15] Haroche S and Raimond J-M 2006 *Exploring the Quantum: Atoms, Cavities and Photons* (Oxford University Press)
[16] Yurke B and Stoler D 1986 Generating quantum mechanical superpositions of macroscopically distinguishable states via amplitude dispersion *Phys. Rev. Lett.* **57** 13
[17] Frattini N E *et al* 2022 The squeezed kerr oscillator: spectral kissing and phase-flip robustness (arXiv:2209.03934 [quant-ph])
[18] Greiner M, Mandel O, Hänsch T W and Bloch I 2002 Collapse and revival of the matter wave field of a Bose–Einstein condensate *Nature* **419** 51
[19] Will S, Best T, Schneider U, Hackermüller L, Lühmann D-S and Bloch I 2010 Time-resolved observation of coherent multi-body interactions in quantum phase revivals *Nature* **465** 197
[20] Vool U and Devoret M 2017 Introduction to quantum electromagnetic circuits *Int. J. Circuit Theory Appl.* **45** 897
[21] Milburn G J 1986 Quantum and classical liouville dynamics of the anharmonic oscillator *Phys. Rev.* A **33** 674
[22] Milburn G J and Holmes C A 1986 Dissipative quantum and classical liouville mechanics of the anharmonic oscillator *Phys. Rev. Lett.* **56** 2237
[23] Zurek W H and Paz J P 1994 Decoherence, chaos and the second law *Phys. Rev. Lett.* **72** 2508
[24] Habib S, Shizume K and Zurek W H 1998 Decoherence, chaos and the correspondence principle *Phys. Rev. Lett.* **80** 4361
[25] Katz I, Retzker A, Straub R and Lifshitz R 2007 Signatures for a classical to quantum transition of a driven nonlinear nanomechanical resonator *Phys. Rev. Lett.* **99** 040404
[26] Katz I, Lifshitz R, Retzker A and Straub R 2008 Classical to quantum transition of a driven nonlinear nanomechanical resonator *New J. Phys.* **10** 125023
[27] Cochrane P T, Milburn G J and Munro W J 1999 Macroscopically distinct quantum-superposition states as a bosonic code for amplitude damping *Phys. Rev.* A **59** 2631
[28] Zhang Y and Dykman M I 2017 Preparing quasienergy states on demand: A parametric oscillator *Phys. Rev.* A **95** 053841
[29] Puri S, Boutin S and Blais A 2017 Engineering the quantum states of light in a kerr-nonlinear resonator by two-photon driving *npj Quantum Inf.* **3** 1
[30] Marthaler M and Dykman M I 2007 Quantum interference in the classically forbidden region: a parametric oscillator *Phys. Rev.* A **76** 010102
[31] Ruiz D, Gautier R, Guillaud J and Mirrahimi M 2023 Two-photon driven kerr quantum oscillator with multiple spectral degeneracies *Phys. Rev.* A **107** 042407
[32] Venkatraman J, Cortinas R G, Frattini N E, Xiao X and Devoret M H 2022 Quantum interference of tunneling paths under a double-well barrier (arXiv:2211.04605)
[33] Carmichael H 1999 *Statistical Methods in Quantum Optics 1: Master Equations and Fokker-Planck Equations* vol 1 (Springer Science & Business Media)
[34] Atalaya J, Kenny T W, Roukes M and Dykman M 2016 Nonlinear damping and dephasing in nanomechanical systems *Phys. Rev.* B **94** 195440
[35] This mechanical photon is also referred to as *phonon*
[36] Hillery M, O'Connell R, Scully M and Wigner E 1984 Distribution functions in physics: fundamentals *Phys. Rep.* **106** 121

[37] Curtright T L, Fairlie D B and Zachos C K 2013 *A Concise Treatise on Quantum Mechanics in Phase Space* (World Scientific Publishing Company)

[38] In dimensionful coordinates it reads $f\star g\equiv f e^{\frac{i\hbar}{2}\left(\overleftarrow{\partial}_x\overrightarrow{\partial}_p-\overleftarrow{\partial}_p\overrightarrow{\partial}_x\right)}g=fg+\frac{i\hbar}{2}\{f,g\}+\mathcal{O}(\hbar^2)$

[39] For example, considering the fluctuation-dissipation associated with a viscous force opposing momentum $F\propto -p$ in a mechanical particle [115], or dielectric loss in quantum circuits. The symmetrization of equation (3) exposes *the photon* for which a symmetrization of x and p has been made. This is justified in the high quality factor limit where x and p are exchanged many times before any appreciable fraction of the *energy* is lost

[40] Romero-Isart O 2011 Quantum superposition of massive objects and collapse models *Phys. Rev.* A **84** 052121

[41] Roda-Llordes M, Candoli D, Grochowski P T, Riera-Campeny A, Agrenius T, García-Ripoll J J, Gonzalez-Ballestero C and Romero-Isart O 2023 Numerical simulation of large-scale nonlinear open quantum mechanics (arXiv:2306.09083)

[42] Without loss of generality we take V to be purely nonlinear, absorbing any quadratic contribution in ω_a

[43] Fröwis F, Sekatski P, Dür W, Gisin N and Sangouard N 2018 Macroscopic quantum states: Measures, fragility and implementations *Rev. Mod. Phys.* **90** 025004

[44] Zurek W H 2001 Sub-planck structure in phase space and its relevance for quantum decoherence *Nature* **412** 712

[45] See [116] for a method to enhance nonlinearities with active driving

[46] Vogel K and Risken H 1989 Quasiprobability distributions in dispersive optical bistability *Phys. Rev.* A **39** 4675

[47] We would like to clarify that this is true in absence of a 'gap' stabilizing the state. Such gap can be Hamiltonian, dissipative or generated by active quantum error correction. In other words, it is possible today to stabilize complicated quantum states [117]. In particular, for the stabilization of any state appearing during the free Kerr evolution of a coherent state see [118]

[48] Since the Hilbert space method is more numerically efficient than the phase space method, the dynamics here shown have been computed using the matrix methods in the qutip package [119]. One hundred states in the Fock basis ensured convergence. It is likely that numerical convenience explains the historical success of Hilbert space methods, in spite of obscuring the quantum-classical correspondence. For numerical considerations in solving the Lindblad equation in phase space see the recent work in [41, 120]

[49] Case W B 2008 Wigner functions and weyl transforms for pedestrians *Am. J. Phys.* **76** 937

[50] Using that the inter-fringe distance of the cat's Wigner function (their period) is $\pi/2|\alpha|$ [15], and that $|W(\beta)|\leqslant 2/\pi$, a back-of-the-envelope calculation to estimate the concavity at the mid-fringe yields the diffusion rate estimate of $\frac{\kappa}{4}|\partial^2_{\beta\beta^*}W|\approx\frac{64}{\pi^3}\kappa|\alpha|^2\approx 2.06\kappa|\alpha|^2$

[51] Note that the regime $\kappa\gg K, +.2777em\omega_a$ is the limit of Aristotelian physics were the system has a strong tendency to its 'rest state' (overdamped). Newton's abstraction was to understand the role of dissipation and imagine a dissipationless system (underdamped, $\kappa\to 0$). It is interesting to think that Newton, having found a set of rules that governed celestial bodies and worldly objects (like apples) alike, had reasons to ignore the role of size, and thus his abstraction lead to the laws of classical physics. We see that taking the limits of $\kappa\to 0$ and 'size'$\to\infty$ in the right order, quantum mechanics survives instead. We call the reader's attention to the following: the laws of classical physics can be recovered from the quantum Moyal bracket, but not the other way around. Quantization procedures are doomed to fail due to Groenwold's theorem [37, 121]

[52] In three dimensions, the Gaussian potential reads $V(\rho,Z)=-V_0\left(\frac{w_0}{w(Z)}\right)^2\exp\left(\frac{-2\rho^2}{w(Z)^2}\right)$, where Z is the position of the atom along the laser propagation axis, and $w(Z)=w_0\sqrt{1+(Z/Z_R)^2}$ is the Gaussian waist of the laser beam, where $Z_R=\pi w_0^2/\lambda$ is the Rayleigh length of the beam. The origin of the coordinates is placed at the focal point of the beam. We compute the small oscillation frequency and the nonlinearity along the radial direction (ρ) to be $\omega_\rho=\sqrt{\frac{4V_0}{mw_0^2}}$ and $k_{4,\rho}=-\frac{2V_0}{w_0^4}<0$. The longitudinal trap properties are $\omega_z^2=\omega_\rho^2 w_0^2/2Z_R^2$ and $k_{4,z}=k_{4,\rho}w_0^4/2Z_R^4$. We consider only the radial properties in the main text $(\rho,Z\to X,0)$ since $k_{4,z}/k_{4,\rho}\ll 1$ for a diffraction-limited waist of $w_0=\lambda/\pi\,\mathrm{NA}=\lambda/2$.

[53] Frimmer M *et al* 2019 Rapid flipping of parametric phase states *Phys. Rev. Lett.* **123** 254102

[54] Vijayan J, Zhang Z, Piotrowski J, Windey D, van der Laan F, Frimmer M and Novotny L 2022 Scalable all-optical cold damping of levitated nanoparticles *Nat. Nanotechnol.* **1 49–54**

[55] In these systems it is possible to cool the particle close to its ground state. Coherent states are generated by an ordinary displacement i.e. displacing the trap, or by resonantly modulating it

[56] Novotny L 2017 Radiation damping of a polarizable particle *Phys. Rev.* A **96** 032108

[57] Regal C, Teufel J and Lehnert K 2008 Measuring nanomechanical motion with a microwave cavity interferometer *Nat. Phys.* **4** 555

[58] Chu Y, Kharel P, Renninger W H, Burkhart L D, Frunzio L, Rakich P T and Schoelkopf R J 2017 Quantum acoustics with superconducting qubits *Science* **358** 199

[59] Reed A *et al* 2017 Faithful conversion of propagating quantum information to mechanical motion *Nat. Phys.* **13** 1163

[60] Chamberland C *et al* 2020 Building a fault-tolerant quantum computer using concatenated cat codes (arXiv:2012.04108)

[61] O'Connell A D *et al* 2010 Quantum ground state and single-phonon control of a mechanical resonator *Nature* **464** 697

[62] Samanta C *et al* 2023 Nonlinear nanomechanical resonators approaching the quantum ground state *Nat. Phys.* **19** 1340–4

[63] Schymik K-N, Pancaldi S, Nogrette F, Barredo D, Paris J, Browaeys A and Lahaye T 2021 Single atoms with 6000-second trapping lifetimes in optical-tweezer arrays at cryogenic temperatures *Phys. Rev. Appl.* **16** 034013

[64] Brown M, Muleady S, Dworschack W, Lewis-Swan R, Rey A, Romero-Isart O and Regal C 2023 Time-of-flight quantum tomography of an atom in an optical tweezer *Nat. Phys.* **19** 569–73

[65] Ravon B 2023 *Phys. Rev. Lett.* **131** 093401

[66] Steck D A 2007 *Quantum and Atom Optics* (available at: https://atomoptics.uoregon.edu/~dsteck/teaching/quantum-optics/)

[67] Note that NA ≈ 0.7 [122] and even NA ≈ 0.9 [123] have been demonstrated in setups like the one required here

[68] Note that, in the pursuit of large nonlinearities (and low photon scattering rates), using short-wavelength 'blue traps' (where the atom behaves as a low intensity seeker) and super-resolution techniques (like using high-order Laguerre-Gauss beams) will provide an experimental edge

[69] Schaetz T 2017 Trapping ions and atoms optically *J. Phys. B: At. Mol. Opt. Phys.* **50** 102001

[70] Stobińska M, Villar A S and Leuchs G 2011 Generation of kerr non-gaussian motional states of trapped ions *Europhys. Lett.* **94** 54002

[71] The Larmor radiation being negligible does not limit the quality factor of the oscillator

[72] Albert V V 2022 Bosonic coding: introduction and use cases (arXiv:2211.05714)

[73] Cai W, Ma Y, Wang W, Zou C-L and Sun L 2021 Bosonic quantum error correction codes in superconducting quantum circuits *Fundam. Res.* **1** 50

[74] Bloch I, Dalibard J and Zwerger W 2008 Many-body physics with ultracold gases *Rev. Mod. Phys.* **80** 885
[75] We note that the experiment could be done with a condensate of atoms, provided the interactions are negligible. This will yield an important gain in the signal-to-noise ratio of the experiment. Studying the effect of quantum statistics in these dynamics could be an interesting avenue
[76] Marklund M and Shukla P K 2006 Nonlinear collective effects in photon-photon and photon-plasma interactions *Rev. Mod. Phys.* **78** 591
[77] Xiao X, Venkatraman J, Cortiñas R G, Chowdhury S and Devoret M H 2023 A diagrammatic method to compute the effective hamiltonian of driven nonlinear oscillators (arXiv:2304.13656)
[78] Wielinga B and Milburn G J 1993 Quantum tunneling in a kerr medium with parametric pumping *Phys. Rev.* A **48** 2494
[79] Goto H 2019 Quantum computation based on quantum adiabatic bifurcations of kerr-nonlinear parametric oscillators *J. Phys. Soc. Japan* **88** 061015
[80] Venkatraman J, Xiao X, Corti nas R G, Eickbusch A and Devoret M H 2022 Static effective hamiltonian of a rapidly driven nonlinear system *Phys. Rev. Lett.* **129** 100601
[81] Marthaler M and Dykman M I 2006 Switching via quantum activation: a parametrically modulated oscillator *Phys. Rev.* A **73** 042108
[82] Dykman M 2012 *Fluctuating Nonlinear Oscillators: From Nanomechanics to Quantum Superconducting Circuits* (Oxford University Press)
[83] The Hilbert space argument can be found in [124] and reduces to $\hat{H}|\pm\alpha\rangle = 0$ with $\hat{H} = -K(\hat{a}^{\dagger 2} - \frac{\epsilon_2}{K})(\hat{a}^2 - \frac{\epsilon_2}{K})$. In phase space, the condition $\hat{a}|\alpha\rangle\langle\alpha| = \alpha|\alpha\rangle\langle\alpha|$ translates to $a \star W_\alpha(x,p) = \alpha W_\alpha(x,p)$ as one can readily verify. Here we use $a = (x+ip)/\sqrt{2}$, $\alpha = (x_0 + ip_0)/\sqrt{2}$ and $W_\alpha(x,p) = e^{-}/\pi$
[84] Since equation (17) is negative semidefinite, the zero eigenvalues bound the spectrum and sets the ground state
[85] Mirrahimi M, Leghtas Z, Albert V V, Touzard S, Schoelkopf R J, Jiang L and Devoret M H 2014 Dynamically protected cat-qubits: a new paradigm for universal quantum computation *New J. Phys.* **16** 045014
[86] Grimm A, Frattini N E, Puri S, Mundhada S O, Touzard S, Mirrahimi M, Girvin S M, Shankar S and Devoret M H 2020 Stabilization and operation of a kerr-cat qubit *Nature* **584** 205
[87] Roberts D and Clerk A A 2020 Driven-dissipative quantum kerr resonators: New exact solutions, photon blockade and quantum bistability *Phys. Rev.* X **10** 021022
[88] Grossmann F, Dittrich T, Jung P and Hänggi P 1991 Coherent destruction of tunneling *Phys. Rev. Lett.* **67** 516
[89] Lignier H, Sias C, Ciampini D, Singh Y, Zenesini A, Morsch O and Arimondo E 2007 Dynamical control of matter-wave tunneling in periodic potentials *Phys. Rev. Lett.* **99** 220403
[90] Tomsovic S and Ullmo D 1994 Chaos-assisted tunneling *Phys. Rev.* E **50** 145
[91] Hensinger W K, Häffner H, Browaeys A, Heckenberg N R, Helmerson K, McKenzie C, Milburn G J, Phillips W D, Rolston S L and Rubinsztein-Dunlop H *et al* 2001 Dynamical tunnelling of ultracold atoms *Nature* **412** 52
[92] Roda-Llordes M, Riera-Campeny A, Candoli D, Grochowski P T and Romero-Isart O 2023 Macroscopic quantum superpositions in a wide double-well potential (arXiv:2303.07959)
[93] Dalibard J and Cohen-Tannoudji C 1985 Dressed-atom approach to atomic motion in laser light: the dipole force revisited *J. Opt. Soc. Am.* B **2** 1707
[94] Lami L, Regula B, Wang X, Nichols R, Winter A and Adesso G 2018 Gaussian quantum resource theories *Phys. Rev.* A **98** 022335
[95] Zurek W H 2003 Decoherence and the transition from quantum to classical—revisited (arXiv:quant-ph/0306072)
[96] Cohen S R and Thompson J D 2021 Quantum computing with circular rydberg atoms *PRX Quantum* **2** 030322
[97] Cong I, Levine H, Keesling A, Bluvstein D, Wang S-T and Lukin M D 2022 Hardware-efficient, fault-tolerant quantum computation with rydberg atoms *Phys. Rev.* X **12** 021049
[98] Nguyen T L *et al* 2018 Towards quantum simulation with circular rydberg atoms *Phys. Rev.* X **8** 011032
[99] Méhaignerie P 2023 *Phys. Rev.* A **107** 063106
[100] Rondin L, Gieseler J, Ricci F, Quidant R, Dellago C and Novotny L 2017 Direct measurement of kramers turnover with a levitated nanoparticle *Nat. Nanotechnol.* **12** 1130
[101] Steck D A, Oskay W H and Raizen M G 2001 Observation of chaos-assisted tunneling between islands of stability *Science* **293** 274
[102] Hensinger W K, Heckenberg N R, Milburn G J and Rubinsztein-Dunlop H 2003 Experimental tests of quantum nonlinear dynamics in atom optics *J. Opt. B: Quantum Semiclass. Opt.* **5** R83
[103] Arnal M, Chatelain G, Martinez M, Dupont N, Giraud O, Ullmo D, Georgeot B, Lemarié G, Billy J and Guéry-Odelin D 2020 Chaos-assisted tunneling resonances in a synthetic floquet superlattice *Sci. Adv.* **6** eabc4886
[104] Chàvez-Carlos J, Cortiñas R G, Reynoso M A P, García-Mata I, Batista V S, Pérez-Bernal F, Wisniacki D A and Santos L F 2023 Driving superconducting qubits into chaos (arXiv:2310.17698)
[105] Wang Z, Pechal M, Wollack E A, Arrangoiz-Arriola P, Gao M, Lee N R and Safavi-Naeini A H 2019 Quantum dynamics of a few-photon parametric oscillator *Phys. Rev.* X **9** 021049
[106] Cortiñas R 2023 Threading an atom with light *Phys. Rev.* A **109** L011102
[107] Puri S *et al* 2020 Bias-preserving gates with stabilized cat qubits *Sci. Adv.* **6** eaay5901
[108] Darmawan A S, Brown B J, Grimsmo A L, Tuckett D K and Puri S 2021 Practical quantum error correction with the XZZX Code and Kerr-Cat Qubits *PRX Quantum* **2** 030345
[109] Dykman M, Bruder C, Lörch N and Zhang Y 2018 Interaction-induced time-symmetry breaking in driven quantum oscillators *Phys. Rev.* B **98** 195444
[110] Chàvez-Carlos J, Lezama T L M, Cortiñas R G, Venkatraman J, Devoret M H, Batista V S, Pérez-Bernal F and Santos L F 2022 Spectral kissing and its dynamical consequences in the squeezed kerr-nonlinear oscillator (arXiv:2210.07255)
[111] Reynoso M A P, Nader D J, Chàvez-Carlos J, Ordaz-Mendoza B E, Cortiñas R G, Batista V S, Lerma-Hernàndez S, Pérez-Bernal F and Santos L F 2023 Quantum tunneling and level crossings in the squeeze-driven kerr oscillator (arXiv:2305.10483)
[112] Iachello F, Cortiñas R G, Pérez-Bernal F and Santos L F 2023 Symmetries of the squeeze-driven kerr oscillator (arXiv:2310.09245)
[113] Wang Q-W and Wu S 2020 Excited-state quantum phase transitions in kerr nonlinear oscillators *Phys. Rev.* A **102** 063531
[114] Caprio M, Cejnar P and Iachello F 2008 Excited state quantum phase transitions in many-body systems *Ann. Phys., NY* **323** 1106
[115] Dalibard J 2015 Une brève histoire des atomes froids *Cours du College de France* **143** ch3
[116] Eickbusch A, Sivak V, Ding A Z, Elder S S, Jha S R, Venkatraman J, Royer B, Girvin S, Schoelkopf R J and Devoret M H 2022 Fast universal control of an oscillator with weak dispersive coupling to a qubit *Nat. Phys.* **18** 1464
[117] Sivak V V *et al* 2022 Real-time quantum error correction beyond break-even **616** 50–55

[118] Sarlette A, Raimond J M, Brune M and Rouchon P 2011 Stabilization of nonclassical states of the radiation field in a cavity by reservoir engineering *Phys. Rev. Lett.* **107** 010402
[119] Johansson J R, Nation P D and Nori F 2012 Qutip: an open-source python framework for the dynamics of open quantum systems *Comput. Phys. Commun.* **183** 1760
[120] Propp T B, Ray S, DeBrota J B, Albash T and Deutsch I 2023 Decoherence limits the cost to simulate an anharmonic oscillator (arXiv:2307.00748)
[121] Groenewold H J 1946 On the principles of elementary quantum mechanics *On the Principles of Elementary Quantum Mechanics* (Springer) pp 1–56
[122] Young A W, Eckner W J, Milner W R, Kedar D, Norcia M A, Oelker E, Schine N, Ye J and Kaufman A M 2020 Half-minute-scale atomic coherence and high relative stability in a tweezer clock *Nature* **588** 408
[123] Robens C, Brakhane S, Alt W, Kleißler F, Meschede D, Moon G, Ramola G and Alberti A 2017 High numerical aperture (na = 0.92) objective lens for imaging and addressing of cold atoms *Opt. Lett.* **42** 1043
[124] Puri S, Grimm A, Campagne-Ibarcq P, Eickbusch A, Noh K, Roberts G, Jiang L, Mirrahimi M, Devoret M H and Girvin S M 2019 Stabilized cat in a driven nonlinear cavity: A fault-tolerant error syndrome detector *Phys. Rev.* X **9** 041009